DRAFT FEB 16, 2012
Preprint typeset using LaTeX style emulateapj v. 08/13/06

SYNCHROTRON SPECTRAL CURVATURE FROM 22 MHZ TO 23 GHZ

A. KOGUT[1]

Draft Feb 16, 2012

ABSTRACT

We combine surveys of the radio sky at frequencies 22 MHz to 1.4 GHz with data from the ARCADE-2 instrument at frequencies 3 to 10 GHz to characterize the frequency spectrum of diffuse synchrotron emission in the Galaxy. The radio spectrum steepens with frequency from 22 MHz to 10 GHz. The projected spectral index at 23 GHz derived from the low-frequency data agrees well with independent measurements using only data at frequencies 23 GHz and above. Comparing the spectral index at 23 GHz to the value from previously published analyses allows extension of the model to higher frequencies. The combined data are consistent with a power-law index $\beta = -2.64 \pm 0.03$ at 0.31 GHz, steepening by an amount $\Delta\beta = 0.07$ every octave in frequency. The observed synchrotron spectral steepening agrees with measurement of the cosmic ray energy spectrum and allows extrapolation of synchrotron emission to frequencies 100 GHz.

Subject headings: radio continuum: general, radiation mechanisms: non-thermal

1. INTRODUCTION

Synchrotron emission from relativistic cosmic ray electrons accelerated in the Galactic magnetic field dominates the diffuse radio continuum at frequencies below 1 GHz. It is an important foreground contaminant for measurements of the cosmic microwave background radiation, and also serves to probe the Galactic magnetic field and cosmic ray distributions. Measurements of the synchrotron frequency spectrum are thus of interest to several areas in astrophysics.

An isotropic distribution of relativistic electrons at a single energy $E = \gamma mc^2$ propagating in a uniform magnetic field B has emissivity

$$\epsilon(\nu) = \frac{\sqrt{3}e^3}{mc^2} B \sin\alpha F(x) \ , \tag{1}$$

where α is the pitch angle between the magnetic field and the line of sight, and

$$F(x) = x \int_x^\infty K^{5/3}(x\prime) dx\prime \tag{2}$$

is defined in terms of the modified Bessel function of order 5/3 with variable $x = \nu/\nu_c$ and

$$\nu_c = \frac{3}{4\pi} \frac{e}{mc} \gamma^2 B \sin\alpha \tag{3}$$

(Schwinger 1949; Westfold et al. 1959; Oster 1961). For a power-law distribution of electron energies $N(E) \propto E^p$ propagating in a uniform magnetic field, the synchrotron emission is also a power law,

$$T_A(\nu) \propto \nu^\beta \tag{4}$$

where T_A is antenna temperature, ν is the radiation frequency, and

$$\beta = \frac{p-3}{2} \tag{5}$$

(Rybicki & Lightman 1979).

Electronic address: Alan.J.Kogut@nasa.gov
[1] Code 665, Goddard Space Flight Center, Greenbelt, MD 20771

Measurements of the synchrotron spectral index provide important input for models of cosmic ray propagation. Solar modulation reduces the local cosmic ray electron density for electron energies below a few GeV so that synchrotron emission provides the most direct probe of low-energy cosmic rays. Measurements of the cosmic ray spectrum above a few GeV in turn inform models of the high-frequency synchrotron spectrum. Energy losses from cosmic ray propagation steepen the cosmic ray spectrum, increasing p toward higher energies. The observed steepening from $p \sim -2.6$ at 5 GeV to $p \sim -3.2$ at 50 GeV predicts a corresponding steepening in the synchrotron spectrum from $\beta \sim -2.8$ at 1 GHz to $\beta \sim -3.1$ at 100 GHz (Strong, Moskalenko, & Ptuskin 2007).

Comparison of the cosmic ray spectra to the predicted synchrotron spectrum is complicated by confusion from competing radio emission sources. The diffuse radio continuum is a superposition of the cosmic microwave background, synchrotron emission, free-free emission from the warm ionized interstellar medium, and thermal emission from interstellar dust. Electric dipole emission from a population of small spinning dust grains contributes an additional signal peaking at frequencies near 20 GHz (Draine & Lazarian 1998; Ali-Haïmoud et al. 2009; Hoang, Draine, & Lazarian 2010; Ysard & Verstraete 2010). A number of authors have attempted to disentangle the various emission sources to determine the synchrotron spectral index (for a recent review see Appendix A of Strong, Orlando, & Jaffe (2011)). Despite some discrepant results, the general trend shows a steepening of the synchrotron spectrum from $\beta \sim -2.5$ at 22 MHz to $\beta \sim -3.0$ above 23 GHz, in rough agreement with the observed cosmic ray spectra.

Several factors contribute to the observed scatter in estimates of the synchrotron spectral index. Most estimates, particularly those below 23 GHz, assume a power-law spectrum for synchrotron and do not explicitly model spectral steepening. Comparisons between closely-separated frequencies more accurately reflect the local synchrotron spectrum, but have larger uncertainties from competing emission sources or measurement offsets. Analyses with broader frequency coverage reduce

foreground and offset uncertainties but average over any spectral steepening.

Two additional effects are important for analyses including data from the Wilkinson Microwave Anisotropy Probe (WMAP) at frequencies 23 to 94 GHz. A growing body of evidence suggests that a substantial fraction of the diffuse continuum near 23 GHz consists of electric dipole radiation from a population of small, rapidly spinning dust grains (Kogut et al. 1996; de Oliveira-Costa et al. 1997, 2004; Miville-Deschênes et al. 2008; Dobler & Finkbeiner 2008; Ysard, Miville-Deschênes, & Verstraete 2010; Kogut et al. 2011; Gold et al. 2011; Planck collaboration 2011). Analyses that ignore this component tend to over-predict the synchrotron amplitude near 23 GHz, biasing the derived spectral index to flatter values when comparing to lower frequencies and steeper values when comparing to higher frequencies.

A second systematic error can result from improper treatment of offsets in the data. Measurements from radio surveys at frequencies below 20 GHz include the absolute intensity (zero level) of the sky. The WMAP differential radiometers are insensitive to any constant (monopole) intensity on the sky; the zero level of the WMAP sky maps is set so that the map intensity in the Galactic polar caps matches a cosecant fit to the mid-latitude sky (Bennett et al. 2003; Hinshaw et al. 2009). Analyses that directly compare low-frequency radio surveys to the WMAP data without subtracting a monopole component from the radio data will miss the corresponding emission in the WMAP bands, biasing the derived spectral index to steeper values.

The zero level bias can be significant. The Haslam et al. (1981) survey at 408 MHz is commonly used to model synchrotron emission. The North Galactic pole has measured temperature 19 ± 3 K at 408 MHz, while a $\csc|b|$ fit to the same 408 MHz map predicts a polar contribution of only 5.1 ± 0.6 K. Similar results apply to the Southern hemisphere, where the measured polar cap temperature of 21 ± 3 K significantly exceeds the value 4.0 ± 0.5 K obtained from a $\csc|b|$ fit. Only 2.7 K of the difference can be attributed to emission from the cosmic microwave background, leaving a large residual.

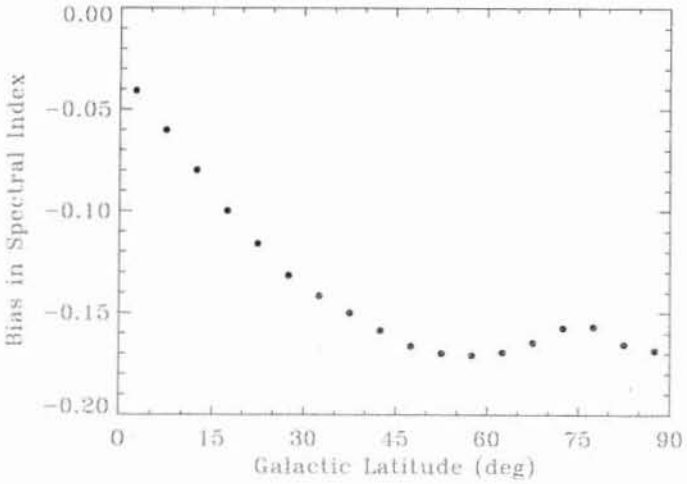

FIG. 1.— Toy model showing effect of improper zero level subtraction on the derived spectral index between 408 MHz and 23 GHz.

TABLE 1
SKY SURVEYS USED FOR SYNCHROTRON ANALYSIS

Frequency (GHz)	Calibration Uncertainty	Offset Uncertainty (K)	Relative Uncertainty[a]
0.022	0.05	5000	0.15
0.045	0.10	250	0.11
0.408	0.10	3.0	0.17
1.420	0.05	0.5	0.63
3.20	0.001	0.011	0.10
3.41	0.001	0.006	0.07
7.98	0.001	0.036	0.89
8.33	0.001	0.042	2.64
9.72	0.001	0.003	0.34
10.49	0.001	0.002	0.27

[a]Quadrature sum of calibration and offset uncertainties, divided by the mid-latitude sky temperature.

Figure 1 illustrates the bias induced by including this residual at 408 MHz but excluding it from the WMAP data. We take the 408 MHz map, remove the 2.7 K CMB monopole, and scale the remaining radio emission to 23 GHz using a power-law index $\beta = -2.7$. We then remove a monopole from the scaled map so that the map temperature in the south polar cap matches the $\csc|b|$ fit. We compute the bias in apparent spectral index by comparing the 408 MHz map to the scaled 23 GHz map before and after removing the scaled monopole. Figure 1 shows the bias in spectral index at 23 GHz, binned by Galactic latitude. Dis-similar treatment of the map zero level creates a spatially varying bias $\Delta\beta \approx 0.15$, comparable to the total spectral steepening predicted by the measured cosmic ray spectra. The bias is largest in regions where the sky brightness is faintest, at high latitudes or away from the Galactic center.

Measurement uncertainties in the absolute level of the sky brightness can also introduce bias in estimates of the synchrotron spectral index. Many of the low-frequency surveys have uncertainty in the measured zero level approaching 30% of the polar cap brightness. As with the toy model above, such measurement errors introduce spatially dependent biases that are largest where the sky brightness is faintest. Minimizing uncertainty in the derived synchrotron spectrum requires a combination of measurements with good sky coverage and good control of offset uncertainty at frequencies where competing emission sources are faint. No such ideal data set yet exists. In this paper, we model the synchrotron spectral index and curvature using low-frequency radio surveys with high sky coverage but large offset uncertainty, combined with higher-frequency measurements with limited sky coverage but excellent offset uncertainty.

2. SKY MAPS

We model synchrotron emission using radio surveys at 22 MHz (Roger et al. 1999), 45 MHz (Maeda et al. 1999; Alvarez et al. 1997), 408 MHz (Haslam et al. 1981), and 1420 MHz (Reich, Testori, & Reich 2001; Reich & Reich 1986). These surveys have full or nearly-full sky coverage at frequencies where Galactic radio emission is significant, with gain and zero-level systematics controlled at the 10–20% level. We supplement the radio surveys with sky maps from the Absolute Radiometer for Cosmology, Astrophysics, and Diffuse Emission (ARCADE

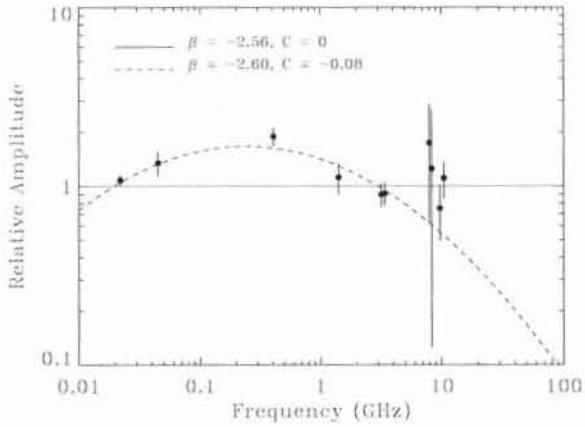

FIG. 2.— Sky temperatures and best-fit model (dashed line) for a 4° diameter patch on the Galactic plane centered on the the brightest pixels in the ARCADe 2 sky coverage. For clarity, the data are plotted relative to the best-fit power-law model ($\beta = -2.56$) with zero curvature (solid line). All fits include the non-trivial covariance between individual data points. The data are well described by a model with spectral index $\beta = -2.60 \pm 0.04$ and curvature $C = -0.081 \pm 0.028$.

2) instrument[2] at 3, 8, and 10 GHz (Kogut et al. 2011). The ARCADE 2 data observe both the Galactic plane and mid-latitude regions ($|b| < 40°$) with sufficient control of zero-level uncertainty to constrain the synchrotron curvature relative to the lower-frequency radio surveys.

Table 1 summarizes the input sky maps. The increase in the offset uncertainty at low frequency is compensated by a corresponding increase in sky brightness. The final column shows the relative measurement uncertainty for a mid-latitude region, defined as the ratio of the combined offset and calibration uncertainty to the measured brightness at $(l, b) = (17°, -35°)$ after removing the CMB monopole. The selected maps provide roughly uniform relative sensitivity to synchrotron emission over 2.5 decades of frequency.

We convert all maps to units of antenna temperature and subtract the CMB monopole at (thermodynamic) temperature 2.725 K from the measured sky temperatures. We then convolve each map to the 11°.6 angular resolution of the ARCADE 2 instrument. At frequencies of 10 GHz and below, both thermal dust emission and spinning dust emission are negligible. Free-free emission, however, can still be appreciable. We correct the convolved maps by scaling the WMAP 7-year maximum entropy free-free model (Gold et al. 2011) to each frequency using spectral index −2.15, convolving the scaled model to 11°.6 angular resolution, and subtracting the convolved model from each sky survey. The resulting maps are dominated by synchrotron emission.

3. ANALYSIS

The input sky maps define a data set $T(\hat{n}, \nu)$ sampled at discrete pixel directions $\hat{n}$ and 10 discrete frequencies ν ranging from 22 MHz to 10 GHz. We model synchrotron emission as a modified power law

$$T(\hat{n}, \nu) = A(\hat{n}) \left(\frac{\nu}{\nu_0}\right)^{\beta + C \ln(\nu/\nu_0)} \quad (6)$$

with spectral curvature C defined with respect to reference frequency $\nu_0 = 310$ MHz. The adopted value for ν_0 minimizes covariance between the fitted amplitude A and spectral index β, simplifying extrapolation to other frequencies.

For each pixel $\hat{n}$ we define a 10 by 10 data covariance matrix M with diagonal elements determined by the instrument noise, calibration and offset uncertainty. The input maps are not all linearly independent. Measurements at 22 MHz used the 408 MHz map to determine the declination dependence of the gain. We estimate the resulting correlation of spatial structure in the two maps at 50%. The ARCADE 2 maps have independent instrument noise but share a fraction of the offset uncertainty related to absolute themometry uncertainty and ground glint (Singal et al. 2011). All 10 maps share a common model for free-free emission. We conservatively estimate the uncertainty in the free-free correction at 30% of the free-free amplitude; however, the results do not change significantly as the model free-free amplitude is varied by as much as 50%. Off-diagonal elements in M include these effects.

We restrict the analysis to the 8% of the sky observed at all 10 frequencies. For each pixel, a least-squares minimization determines the best-fit parameters A, β, and C. Figure 2 shows the measured temperature and best-fit model for the brightest Galactic plane region $(l, b) = (-52°, 0°)$ within the common sky coverage. The data show evidence for spectral curvature, with best-fit values $\beta = -2.60 \pm 0.04$ and $C = -0.081 \pm 0.028$ evaluated at $\nu_0 = 310$ MHz. The spectral curvature C for this region is significant at approximately 3 standard deviations compared to the baseline model with $C = 0$.

We may extrapolate the spectral models to compare the results at frequencies 10 GHz and below to independent determinations of the spectral index using WMAP data at frequencies 23 GHz and above. We compute the antenna temperature of the modeled spectra to derive the effective power-law index for frequencies near 23

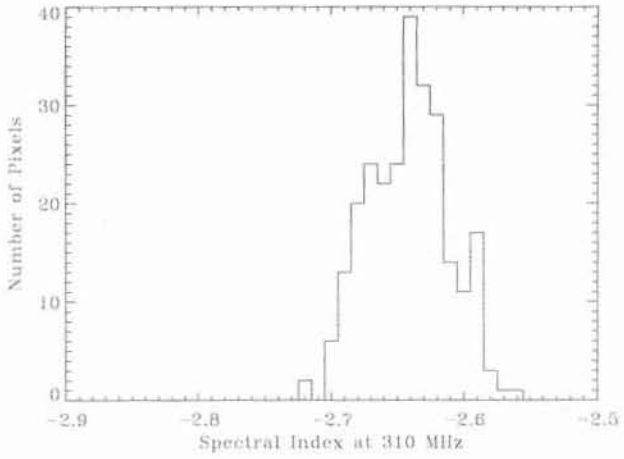

FIG. 3.— Spectral index evaluated at 310 MHz from the 11-frequency fit.

[2] The ARCADE data are available at the Legacy Archive for Microwave Background Data Analysis, http://lambda.gsfc.nasa.gov

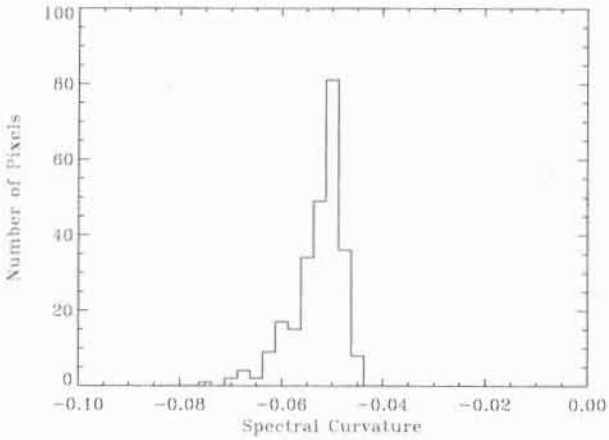

FIG. 4.— Spectral curvature from 11-frequency fit. The mean curvature $C = -0.052$ corresponds to a steepening of the local spectral index by an amount $\Delta\beta = 0.07$ every octave in frequency.

GHz. Note that this is not equivalent to evaluating Eq. 6 at $\nu = 23$ GHz, which would yield the scaling from 310 MHz to 23 GHz but not the power-law index at 23 GHz. The mean for all 258 pixels in the common sky coverage is $\beta_{23} = -3.02$ with standard deviation 0.22.

The extrapolated value compares well with independent determinations of the spectral index above 23 GHz. Kogut et al. (2004) analyze WMAP polarization data to derive synchrotron spectral index $\beta = -3.2 \pm 0.1$ averaged over the full sky. Dunkley et al. (2009) use a Bayesian analysis of polarization data and find the mean spectral index $\beta = -3.03 \pm 0.04$ with pixel-to-pixel standard deviation 0.25 the high-latitude sky. Gold et al. (2011) use template fitting techniques to derive spectral index $\beta = -3.13$ between 23 and 33 GHz.

Much of the scatter in the extrapolated spectral indices results from pixels at high latitude where the emission is faintest. The extrapolated index in these pixels can reach unphysical values. We reduce the scatter by constraining the spectral index at 23 GHz. For each pixel, we use the radio data (Table 1) to fit the synchrotron amplitude $A(\hat{n})$ over a 2-dimensional grid in the spectral parameters β and C. At each grid point, we compute the χ^2 value $R^T M^{-1} R$ where M^{-1} is the inverse covariance matrix and R is the difference vector between the measured and modeled temperatures. We then use the spectral parameters β and C to model the power-law index at 23 GHz and compare the resulting value to a prior. We use the difference between the extrapolated spectral index and the prior to augment the χ^2 at each grid point,

$$\chi^2 \rightarrow \chi^2 + \left(\frac{\beta_{23} - \beta_p}{\sigma_p} \right)^2 , \qquad (7)$$

where β_{23} is the model spectral index evaluated at 23 GHz, and $\beta_p \pm \sigma_p = -3.1 \pm 0.1$ is the prior at 23 GHz. The minimum χ^2 over the entire grid then defines the best-fit model at that pixel. This allows inclusion of the spectral information derived from frequencies above 23 GHz without confusion from either additional emission components (spinning dust) above 23 GHz or the missing zero level in the WMAP data.

Figures 3 and 4 show the distribution of the resulting best-fit values for the spectral index and curvature. Including the constraint at 23 GHz, the best-fit spectral index has mean value -2.64 and standard deviation 0.03 at reference frequency $\nu_0 = 310$ MHz. The best-fit curvature has mean value -0.052 with standard deviation 0.005. The corresponding spectral index at 23 GHz is $\langle \beta_{23} \rangle = -3.09$ with standard deviation 0.05. Inclusion of the prior at 23 GHz does not induce a significant shift in the mean for the extrapolated spectral index, but does significantly reduce the pixel-to-pixel scatter.

4. DISCUSSION

Radio data show statistically significant steepening of the synchrotron spectrum from 22 MHz to 10 GHz. The nearly uniform relative uncertainty of the selected data minimizes dependence of the fitted parameters on offset or calibration errors at any one frequency. We test whether the best-fit parameters are particularly sensitive to any one input map by repeating the analysis after dropping one or two maps from the fit. We select either one radio survey (22 MHz, 45 MHz, 408 MHz, or 1420 MHz) or a pair of ARCADE frequency channels (3 GHz, 8 GHz, or 10 GHz) and repeat the fit after deleting the corresponding elements from the data vector T and covariance matrix M. The resulting shift in either the spectral index or curvature parameters is smaller than the pixel-to-pixel standard deviation using all 10 frequency channels. Systematic errors in the offset or temperature calibration do not appear to dominate the multi-frequency analysis.

The steepening of the synchrotron spectrum is consistent with models of cosmic ray propagation in the Galactic magnetic field. Jaffe et al. (2011) combine radio observations with the GALPROP[3] cosmic ray propagation code to model synchrotron emission on the Galactic plane. They find a power-law index $-2.8 < \beta < -2.74$ from 408 MHz to 2.3 GHz and $-2.98 < \beta < -2.91$ from 2.3 GHz to 23 GHz. The corresponding values for the spectral steepening model are $\beta = -2.76$ from 408 MHz to 2.3 GHz and $\beta = -2.97$ from 2.3 GHz to 23 GHz.

We may use the best-fit values in each pixel to predict the synchrotron spectrum at higher frequencies where the emission is fainter and competing sources stronger. Previous attempts to disentangle competing emission from free-free, synchrotron, thermal dust, and spinning dust emission using WMAP data have suffered from degeneracy between the synchrotron and spinning dust emission, both of which are falling at frequencies above 33 GHz (see, e.g., the discussion in Gold et al. (2011)). Extending the synchrotron curvature observed at lower frequencies into the millimeter band reduces confusion between the spinning dust and synchrotron spectra and may facilitate charcterization of both the spatial distribution and frequency spectrum of spinning dust emission in the interstellar medium.

Table 2 shows the local power-law index $T \propto \nu^\beta$ at selected frequency bands. The modeled spectrum steepens by $\Delta\beta = 0.07$ every octave in frequency, from $\beta = -2.67$ at 408 MHz to $\beta = -3.24$ at 94 GHz. Note, however, that the spectral steepening observed at low frequencies can not continue indefinitely. *Fermi* measurements of the cosmic ray energy spectrum are consistent with a

[3] http://galprop.stanford.edu

TABLE 2
LOCAL POWER-LAW SPECTRAL INDEX

Frequency (GHz)	Power-Law Index
0.408	-2.67
23	-3.09
33	-3.13
41	-3.15
61	-3.19
94	-3.24

single power law from energy 7 GeV to 1 TeV (Abdo et al. 2009; Ackermann et al. 2010, 2012). If anything, the *Fermi* data suggest a modest flattening of the cosmic ray energy spectrum at higher energies, which would induce a positive curvature to the synchrotron spectrum. Direct confirmation of the synchrotron spectrum above 23 GHz remains a challenge.

5. CONCLUSIONS

Radio data are consistent with a synchrotron spectrum that steepens with frequency from 22 MHz to 10 GHz. Direct comparison of low-frequency radio surveys with the WMAP data at 23 to 94 GHz is complicated both by the presence of additional emission components at higher frequencies and by the subtraction of a substantial monopole component of sky emission by the differential WMAP instrument. The synchrotron spectral index at 23 GHz, derived using only lower-frequency radio surveys, is consistent with the value derived independently using only data at higher frequencies. We extend the radio data by comparing the extrapolated index at 23 GHz to a prior based on higher-frequency data. The combined data have mean spectral index $\beta = -2.64 \pm 0.03$ and curvature $C = -0.052 \pm 0.005$ at reference frequency 0.31 GHz. The measured spectrum steepens by an amount $\Delta\beta = 0.07$ every octave in frequency. The observed synchrotron spectral steepening agrees with measurement of the cosmic ray energy spectrum and allows extrapolation of synchrotron emission to frequencies 100 GHz.

This research is based upon work supported by the National Aeronautics and Space Administration through the Science Mission Directorate under the Astronomy and Physics Research and Analysis suborbital program.

REFERENCES

Abdo, A. A., et al., 2009, Phys. Rev. Lett., 102, 181101
Ackermann, M., et al., 2012, Phys. Rev. Lett., 108, 011103
Ackermann, M., et al., 2010, Phys. Rev. D, 82, 092004
Ali-Haïmoud, Y. Hirata, C. M. & Dickinson, C., 2009, MNRAS, 395, 1055
Alvarez, H., Aparici, J., May, J., and Olmos, F., 1997, A&AS, 124, 315
Bennett, C. L., et al., 2003, ApJS, 148, 97
Dobler, G. and Finkbeiner, D. P., 2008, ApJ, 680, 1222
Draine, B. T. and Lazarian, A., 1998, ApJ, 494, L19
Dunkley, J, et al. 2009, ApJ, 701, 1804
Gold, B. et al., 2011, ApJS, 192, 15
Haslam, C. G. T., et al., 1981, A&A, 100, 209
Hinshaw, G., et al., 2009, ApJS, 180, 225
Hoang, T., Draine, B. T., & Lazarian, A., 2010, ApJ, 715, 1462
Jaffe, T. R., et al., 2011, MNRAS, 416, 1152
Kogut, A. et al., 2011, ApJ, 734, 4
Kogut, A. et al., 2004, ApJS, 154, 493
Kogut, A., et al., 1996, ApJ, 460, 1
Maeda, K., Alvarez, H., Aparici, J., May, J., and Reich, P., 1999, A&AS, 140, 145
Miville-Deschênes, M.-A., et al., 2008, A&A, 490, 1093
de Oliveira-Costa, A., et al., 2004, ApJ, 606, L89
de Oliveira-Costa, A., et al., 1997, ApJ, 482, L17
Oster, L., 1961, Phys. Rev., 121, 961
Planck Collaboration, 2011, A&A, 536, A20
Reich, P., Testori, J. C., and Reich, W., 2001, A&A, 376, 861
Reich, P., and Reich, W., 1986, A&AS, 63, 205
Roger, R. S., Costain, C. H., Landecker, T. L., and Swerdlyk, C. M., 1999, A&AS, 137, 7
Rybicki, G. B. & Lightman, A. 1979, Radiative Processes in Astrophysics (Wiley & Sons: New York)
Schwinger, J., 1949, Phys. Rev., 75, 1912
Singal, J. et al., 2011, ApJ, 730, 138
Strong, A. W., Moskalenko, I. V., & Ptuskin, V. S., 2007, Annu. Rev. Nucl. Part. Sci., 57, 285
Strong, A. W., Orlando, E., & Jaffe, T. R., 2007, å, 534, A54
Westfold, K. C., 1959, ApJ, 130, 241
Ysard, N. & Verstraete, L., 2010, A&A, 509, A12
Ysard, N., Miville-Deschênes, M. A., & Verstraete, L., 2010, A&A, 509, L1